

Dalton Transactions

An international journal of inorganic chemistry

Accepted Manuscript

This article can be cited before page numbers have been issued, to do this please use: C. Caporale, A. N. Sobolev, W. Phonsri, K. S. Murray, A. Swain, R. Gopalan, M. I. Ogden, M. Massi and R. O. Fuller, *Dalton Trans.*, 2020, DOI: 10.1039/D0DT02855J.



This is an Accepted Manuscript, which has been through the Royal Society of Chemistry peer review process and has been accepted for publication.

Accepted Manuscripts are published online shortly after acceptance, before technical editing, formatting and proof reading. Using this free service, authors can make their results available to the community, in citable form, before we publish the edited article. We will replace this Accepted Manuscript with the edited and formatted Advance Article as soon as it is available.

You can find more information about Accepted Manuscripts in the [Information for Authors](#).

Please note that technical editing may introduce minor changes to the text and/or graphics, which may alter content. The journal's standard [Terms & Conditions](#) and the [Ethical guidelines](#) still apply. In no event shall the Royal Society of Chemistry be held responsible for any errors or omissions in this Accepted Manuscript or any consequences arising from the use of any information it contains.

ARTICLE

Lanthanoid pyridyl- β -diketonate 'triangles'. New examples of single molecule toroicsReceived 00th January 20xx,
Accepted 00th January 20xxChiara Caporale,^a Alexandre N. Sobolev,^b Wasinee Phonsri,^c Keith S. Murray,^c Abinash Swain,^d Gopalan Rajaraman,^d Mark I. Ogden,^a Massimiliano Massi^a and Rebecca O. Fuller^{a,e*}

DOI: 10.1039/x0xx00000x

Trinuclear lanthanide clusters have been synthesised and investigated as toroidal spin systems. A pyridyl functionalised β -diketonate, 1,3-bis(pyridin-2-yl)propane-1,3-dione (**o-dppdH**) has been used to synthesise a family of clusters of the form $[\text{Dy}_3(\text{OH})_2(\text{o-dppd})_3\text{Cl}_2(\text{H}_2\text{O})_4]\text{Cl}_2 \cdot 7\text{H}_2\text{O}$ (**1**), $[\text{Tb}_3(\text{o-dppd})_3(\mu_3\text{-OH})_2(\text{CH}_3\text{CH}_2\text{OH})_3\text{Cl}_3][\text{Tb}_3(\text{o-dppd})_3(\mu_3\text{-OH})_2(\text{H}_2\text{O})(\text{CH}_3\text{CH}_2\text{OH})_2\text{Cl}_3]\text{Cl}_2 \cdot \text{H}_2\text{O}$ (**2**), $[\text{Ho}_3(\text{OH})_2(\text{o-dppd})_3\text{Cl}(\text{H}_2\text{O})_5]\text{Cl}_3 \cdot 3\text{H}_2\text{O}$ (**3**) and $[\text{Er}_3(\text{OH})_2(\text{o-dppd})_3\text{Cl}_2(\text{H}_2\text{O})_3(\text{CH}_3\text{OH})]\text{Cl}_2 \cdot 3\text{H}_2\text{O} \cdot \text{CH}_3\text{OH}$ (**4**). Despite the previous occurrence of this structural motif in the literature, these systems have not been widely investigated in terms of toroidal behaviour. Magnetic studies were used to further characterise the complexes. DC susceptibility studies support weak antiferromagnetic exchange in the complexes. Slow magnetic relaxation behaviour is observed in the dynamic AC magnetic studies for complex **1**. Theoretical studies predict that complex **1** and **3** have a non-magnetic ground state based on a toroidal arrangement of spins. Changes to the coordination environment in **2** do not support a toroidal spin state. The prolate nature of Er^{III} centres in complex **4** and large transverse anisotropy do not support the toroidal arrangement of lanthanoid spins in the complex.

Introduction

Developing a synthetic methodology to obtain specific lanthanoid clusters for applications such as single molecule magnets (SMMs)^{1, 2} and luminescence^{3, 4} is a major current area of interest.⁵ Understanding how the structure and coordination environment impacts on the measured properties is key for the advancement of these molecules into future applications. β -diketonates are a versatile and highly functionalisable ligand class which have been shown to support polynuclear lanthanoid cluster formation.^{6, 7} Such complexes are normally comprised of a hydroxo-bridged polynuclear lanthanoid cluster core encapsulated by β -diketonate ligands. Examples of mononuclear,^{8, 9} dinuclear,¹⁰ trinuclear¹¹ and larger clusters¹² supported by β -diketonate ligands are known. Coordination with these molecules generally occurs through the bidentate backbone of the β -diketonate ligand together with additional co-ligands contained within the coordination sphere.

Functionalisation of the diketonate scaffold or the addition of co-ligands can be used to alter the coordination environment.^{11, 13}

The wealth of functionalities available for the β -diketonate family provides a good opportunity to develop structural-magnetic property relationships in a family of structures. This statement may at first seem counter intuitive, as the development of lanthanoid SMMs is centred on using the ligand field symmetry to enhance the inherent anisotropy of the Ln^{III} ions with large magnetic moments.^{14, 15} The best examples of Ln -SMMs involve only a single lanthanoid ion (e.g. mononuclear complexes).^{16, 17} Polynuclear Ln complexes usually only display very weak SMM behaviour due to a lack of interaction through μ -bridging between ions.^{18, 19} The lack of exchange and the poor anisotropy does not lead to a stabilisation of a bistable ground state at notable temperatures (with the exception of Dy). However, polynuclear clusters comprised of an appropriate geometry can result in an ideal environment for alternative spin arrangements.²⁰

Triangular spin arrangements are well known avenues for producing interesting properties.²¹ Oxo-bridged transition metal complexes have long been known to exhibit spin frustration.^{22, 23} More recently, triangular Dy_3 cluster complexes have been shown to display a toroidal spin arrangement in these single molecule toroics (SMTs).²⁴ Depending on the type of SMTs, these systems may have a nonmagnetic ground state which exists based on a toroidal arrangement of spins.²⁰ This non-magnetic state does not interact with the applied magnetic field and is observed as a tail in the field dependent magnetisation measurements. These materials have unique spin transport properties based on their strongly anisotropic

^a School of Molecular and Life Sciences, Curtin University, Bentley WA 6102, Australia.

^b School of Molecular Sciences and CMCA, M310, The University of Western Australia, Crawley WA 6009, Australia.

^c School of Chemistry, Monash University, Clayton VIC 3800, Australia

^d Department of Chemistry, Indian Institute of Technology Bombay Powai, Mumbai, Maharashtra, 400076, India

^e School of Natural Sciences-Chemistry, University of Tasmania, Hobart TAS 7001, Australia. E-mail: rebecca.fuller@utas.edu.au

Electronic Supplementary Information (ESI) available: Reaction scheme and characterisation for **o-dppdH** (¹H NMR; ¹³C NMR, IR); Structural representations including packing arrangements and complexes **1-4**; Selected interatomic distances and angles; Polyhedra view complexes **2-4**; magnetic measurements complexes **2-4**; Poly_aniso calculated susceptibility; Dynamic calculations for complex **1** and **4**; Magnetic exchange in complexes **2-4**; Tabulated energies and ground-state g tensors. See DOI: 10.1039/x0xx00000x

nature, resulting in their suitability for a number of potential applications including quantum computers and spintronic devices.^{25, 26} In addition to Dy based SMTs, non-triangular analogues for other lanthanoids have also been recently reported, Ln = Tb, Ho, Er.^{27, 28}

Trigonal Dy₃ complexes provided the first examples of SMTs.²⁹ In these complexes the ring-like arrangement of spins is strongly anisotropic and aligns with the plane of the array. However, as the SMT field has matured, a wealth of structures has been developed.^{27, 30, 31} New examples with a range of structural motifs have been reported, including square,³² wheel,³³ cubane³⁴ and 3*d*-linked pair of Dy₃ heptanuclear clusters.³¹ In this work we have focused on developing complexes with a similar structural motif to the trigonal complexes.^{11, 24}

Pyridyl functionalised β -diketonates have shown potential as supporting ligands for SMTs. The pyridin-4-yl analogue has been used in the synthesis of a cubane-shaped Dy₄ complex.²⁷ A Ho^{III} complex with the bis(pyridin-2-yl) β -diketonate has been shown to consist of a coordination environment similar to *o*-vanillin Dy^{III} triangles which exhibited a toroidal spin arrangement.^{11, 24} Despite the similarity of the core and bridging atoms, the magnetic behaviour exhibited by the holmium complex was distinctly different to the dysprosium system. It was postulated to be likely due to the result of the difference in the magnetic anisotropy of the holmium and dysprosium centres. In this vein we have synthesised a family of triangular molecules based on Dy^{III}, Tb^{III}, Ho^{III} and Er^{III} with the deprotonated 1,3-bis(pyridin-2-yl)propane-1,3-dione (Figure 1) ligand (**o-dppdH**). This family of lanthanide complexes has been used to investigate the role of the lanthanoid centre in the spin structure of the metal core. In this work we aim to further elucidate the impact of the lanthanoid anisotropy on the ligand field and magnetic exchange by undertaking a detailed experimental and theoretical investigation on these systems.

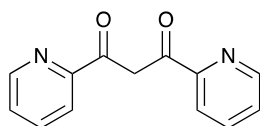


Figure 1: Structure of the **o-dppdH** ligand, 1,3-bis(pyridin-2-yl)propane-1,3-dione.

Results and discussion

Synthesis and characterisation of complexes

A series of trinuclear lanthanoid clusters with the formula [Ln₃(μ_3 -OH)₂(**o-dppd**)₃Cl_xL_y]^{4-x} where Ln= Dy^{III}, Tb^{III}, Ho^{III} or Er^{III}; x+y=6; L = H₂O or CH₃CH₂OH or CH₃OH have been prepared. **o-dppdH** was synthesised via a Claisen condensation of ethyl-2-picolinate and 2-acetylpyridine using a literature procedure (Scheme S1).^{11, 35} The ligand (2 eq.) was treated with a lanthanoid salt of the form LnCl₃·6H₂O (where Ln= Dy^{III}, Tb^{III}, Ho^{III} and Er^{III}) in the presence of triethylamine. Although a stoichiometry of 1:1 appears to be more appropriate for the production of a trigonal system, the 2:1 ratio and complexation proceeding at elevated temperatures was necessary

for the production of these systems. Collection of the product was achieved after a series of washing steps using acetonitrile and pyridine to remove unreacted **o-dppdH** and lanthanoid salt from the target compound. The target clusters were then collected as a powder and crystals suitable for X-ray diffraction were grown using slow evaporation or diffusion techniques. If required, the bulk sample was recrystallised for magnetic measurements as well as analysis.

Crystallography

Figure 2 shows the structure of the complex cation of [Dy₃(OH)₂(**o-dppd**)₃Cl₂(H₂O)₄Cl₂·7H₂O (**1**). The compound crystallises in the triclinic space group $P\bar{1}$. Each of the β -diketonate ligands binds to two of the Dy^{III} centres. One of the oxygens from the β -diketonate binds exclusively to one Dy^{III} atom. The other oxygen is shared (μ_2 -O) between the two centres (Dy-O-Dy angles in the 97.96–98.37° range). The second of the dysprosium centres is also bound to a nitrogen from the pyridyl group, so that each ligand is bound through μ - $\eta^2(N,O); \eta^2(O,O')$ to the lanthanoid centres with the other pyridyl nitrogen atom left unbound. The lanthanoid centres and ligand bridging oxygen atoms form an essentially planar 6 membered ring (deviation 0.06 Å). The metal array approximates an equilateral triangle, with deviation from the ideal Ln-Ln-Ln angle of less than 0.24°. The three eight-coordinate Dy^{III} centres are bridged by two central μ_3 -OH oxygens which lie above and below the metal plane by 1.211 and 1.175 Å, respectively. Two of the Dy^{III} cations are coordinated to chloride anions. The final positions in the Dy^{III} coordination sphere contain H₂O molecules. One of the unbound pyridyl rings is distorted over two positions with occupancies set to 0.6667 and 0.3333. As a result, the neighbouring H₂O contained in the lattice is disordered. Selected bond lengths for all the complexes are given in Table 1 with additional data contained in the ESI (Table S1 and S2).

Using continuous SHAPE measurements, the 8-coordinate environment approximates a triangular dodecahedron (TDD8) with D_{2d} symmetry and based on the shape distortion parameter given in Table 1 for all studied complexes, this is valid for all Ln metal centres.³⁶ The polyhedral representations are given in Figure S3 (ESI)

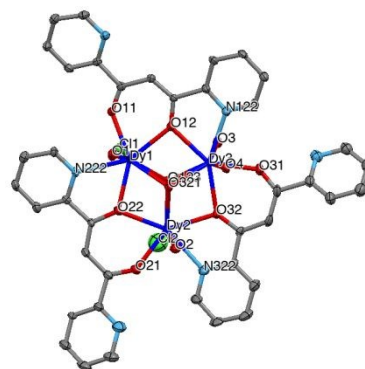


Figure 2: Molecular structure of complex **1**. Dy...Dy distances are 3.54–3.55 Å. Thermal ellipsoids are set to 30 % probability. For clarity, hydrogen atoms and lattice solvent are omitted.

Table 1: Selected interatomic distances and SHAPE parameter for $[\text{Dy}_3(\text{OH})_2(\text{o-dppd})_3\text{Cl}_2(\text{H}_2\text{O})_4]\text{Cl}_2 \cdot 7\text{H}_2\text{O}$ **1**, $\{[\text{Tb}_3(\text{o-dppd})_3(\text{OH})_2(\text{CH}_3\text{CH}_2\text{OH})_3\text{Cl}_3][\text{Tb}_3(\text{o-dppd})_3(\mu_3\text{-OH})_2(\text{H}_2\text{O})(\text{CH}_3\text{CH}_2\text{OH})_2\text{Cl}_3] \cdot 3\text{H}_2\text{O}\}$ **2**, $[\text{Ho}_3(\text{OH})_2(\text{o-dppd})_3\text{Cl}(\text{H}_2\text{O})_5]\text{Cl}_3 \cdot 3\text{H}_2\text{O}$ **3** and $[\text{Er}_3(\text{OH})_2(\text{o-dppd})_3\text{Cl}_2(\text{H}_2\text{O})_3(\text{CH}_3\text{OH})]\text{Cl}_2 \cdot 3\text{H}_2\text{O} \cdot \text{CH}_3\text{OH}$ **4**.

	1			2			3			4		
	Dy1	Dy2	Dy3	Tb1	Tb2	Tb3	Ho1	Ho2	Ho3	Er1	Er2	Er3
distances (Å)												
Ln-Cl	2.644(2)	2.543(6)	-	2.672(1)	2.672(1)	2.712(1)	2.645(4)	-	-	2.577(4)	2.642(1)	-
Ln-O123 ($\mu_3\text{-O}$)	2.394(5)	2.382(6)	2.359(4)	2.390(3)	2.392(3)	2.376(3)	2.383(8)	2.363(8)	2.36(1)	2.353(3)	2.339(3)	2.357(3)
Ln-O321 ($\mu_3\text{-O}$)	2.356(5)	2.350(4)	2.374(6)	2.386(3)	2.397(3)	2.377(3)	2.356(8)	2.354(7)	2.38(1)	2.371(3)	2.373(3)	2.331(3)
Ln-N	2.498(7)	2.486(7)	2.486(7)	2.530(4)	2.522(4)	2.520(3)	2.51(1)	2.50(1)	2.511(9)	2.494(4)	2.498(3)	2.498(3)
Distortion												
SHAPE (D_{2d})*	1.230	0.854	1.033	1.307	1.296	1.571	1.213	0.811	0.985	0.814	1.217	0.901

* D_{2d} symmetry for triangular dodecahedral polyhedral

for complexes **2-4**. The closer the SHAPE index is to zero the less distortion from the ideal environment. The geometry of the Dy^{III} centres in **1** appears to approximate a triangular dodecahedron (TDD8) with D_{2d} symmetry (Figure 3). The metal bond distances and angles for **1** are similar to those in the Dy^{III} *o*-vanillin complexes which have the form $[\text{Dy}_3(\mu_3\text{-OH})_2\text{L}_3\text{Cl}_2(\text{H}_2\text{O})_4]$ where L = 2-hydroxy-3-methoxybenzaldehyde.²⁹ Continuous shape measurements performed on the Dy^{III} *o*-vanillin systems found the geometry of the complexes also approximates a triangular dodecahedron (TDD8) with D_{2d} symmetry. In complex **1**, the lattice contains large voids which are occupied by non coordinated Cl ions and H_2O . The solvent system used to isolate the complex is also shown to impact on the solvent contained within the voids of complex **2** and **4**.

A similar metal array is seen in the $\{[\text{Tb}_3(\text{o-dppd})_3(\mu_3\text{-OH})_2(\text{CH}_3\text{CH}_2\text{OH})_3\text{Cl}_3][\text{Tb}_3(\text{o-dppd})_3(\mu_3\text{-OH})_2(\text{H}_2\text{O})(\text{CH}_3\text{CH}_2\text{OH})_2\text{Cl}_3] \cdot \text{H}_2\text{O}\}$ (**2**), $[\text{Ho}_3(\text{OH})_2(\text{o-dppd})_3\text{Cl}(\text{H}_2\text{O})_5]\text{Cl}_3 \cdot 3\text{H}_2\text{O}$ (**3**) and $[\text{Er}_3(\text{OH})_2(\text{o-dppd})_3\text{Cl}_2(\text{H}_2\text{O})_3(\text{CH}_3\text{OH})]\text{Cl}_2 \cdot 3\text{H}_2\text{O} \cdot \text{CH}_3\text{OH}$ (**4**) complexes (ESI Figure S2). The three lanthanoid centres are in an equilateral arrangement with similar coordination to the β -diketonate ligand and central hydroxide groups as discussed for **1**. Selected bond lengths are given in Table 1 and in the ESI (Table S1 and S2) Depending on the lanthanoid atom, the coordination sphere contains between one and three Cl anions with the other positions consisting of solvent molecules, dependent on the recrystallisation method (H_2O , CH_3OH , $\text{CH}_3\text{CH}_2\text{OH}$). Using continuous SHAPE measurements, the 8-coordinate environment approximates a triangular dodecahedron (TDD8) with D_{2d} symmetry, the polyhedral representations are contained in Figure S3 (ESI). The structure of the holmium analogue (**3**) is distorted in a similar manner to **1**, namely one of the unbound pyridyl rings occurs in two positions (occupancy 0.5) with neighbouring lattice solvent also being disordered.

Using CrystalExplorer 3.1³⁷ the packing arrangement of molecules is found to be influenced by π - π interactions as well as coordinated Cl anions hydrogen bonding to the pyridyl rings on the adjacent molecule and lattice solvent (ESI Figure S1a). The metal arrays are arranged in parallel planes (Figure 4). Intermolecular π stacking interactions between the delocalised diketonate and pyridyl ring or between two adjacent pyridyl rings, with a maximum centroid to centroid distance of 3.9 Å noted in **1** (ESI Figure S1b). The molecules

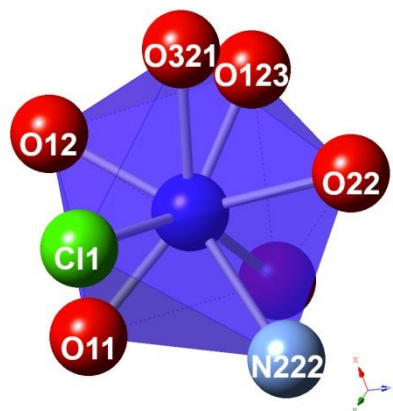


Figure 3: Polyhedral view of the eight coordinate geometry of Dy1 in complex **1** the two $\mu_3\text{-O(H)}$ are positioned above the LnIII centre (O321 and O123). This depiction from CrystalMaker® v9.1.3 supports a TDD-8 coordination environment around the lanthanoid centre. Purple=DyIII, red=O, green=Cl and blue=N atom.

are found to link together through the chloride counter ions and the pyridyl ring with either a coordinated water and/or hydroxide ligands (Figure 4). The hydrogen bond is indirect as it does not occur solely between donor atoms coordinated to the Dy^{III} centres. Rather, it involves both donor and lattice solvent/counter ions. However, since it is the triangular arrangement of the spins and the associated

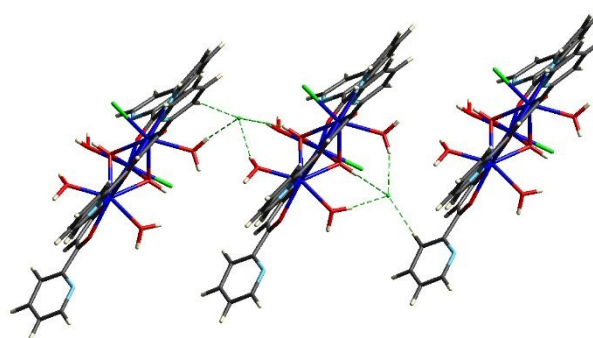


Figure 4: CrystalExplorer 3.1 is used to depict the hydrogen bonding network in **1**. Purple= Dy^{III} , red=O, green=Cl, light blue=N, grey=C and white=H.

anisotropy which impact on the stabilisation of a non-magnetic

toroidal spin states, the extended network will not significantly affect the occurrence of a toroidal state.²⁴

Both lattice and coordinated solvents were impacted by conditions used for crystallisation. When comparing complex **3**, to the previously reported analogue¹¹ an additional water and one less chloride were refined as co-ligands with further water contained in the lattice. In complex **2** the co-ligands are disordered, whereby one of the coordinated H₂O molecules is replaced by a CH₃CH₂OH molecule. To ensure that the variations between reaction batches only represented the slight changes mentioned, two structural analyses for crystals from the erbium system were fully refined. [Er₃(OH)₂(**o-dppd**)₃Cl₂(H₂O)₃(CH₃OH)]Cl₂·5H₂O (**4a**) highlights the variable solvation for different crystallisations. Full details of this complex can be found in the ESI (Table S1) Metal analysis was used to confirm lanthanide content. These results were consistent with the proposed formulations as well as values inferred from the room temperature susceptibility.

The extended structures for complexes **2-4** are dependent on π - π interactions and coordinated Cl anions linked to neighbouring pyridyl rings in the way depicted for complex **1** in Figure S1. The coordination environments in the lanthanoid triangles is different for Tb^{III} but Ho^{III} and Er^{III} are similar to that in Dy^{III}. The linking of the metal arrays for both **3** and **4** is also similar to that seen for complex **1**. In **3**, the Ho^{III} metal array of neighbouring molecules are connected through a hydrogen bonding network involving the lattice Cl anions being linked from a pyridyl ring of one molecule to coordinated H₂O and μ_3 -O of another. In an analogous manner, the complex **4** metal arrays are linked through two slightly different lattice Cl anion environments. The first is identical to that observed in **1** and **3**. The second involves a pyridyl ring and coordinated CH₃CH₂OH from one molecule being linked through the lattice Cl anions to a coordinated H₂O and central μ_3 -O of the neighbouring molecule. A different arrangement is seen for the Tb^{III} metal arrays (**2**). Neighbouring molecules are still linked through lattice Cl anions. However, in this case the coordinated CH₃CH₂OH (or H₂O) groups are also linked with the neighbouring molecule pyridyl, with the central μ_3 -O playing no role. In the absence of coordinated CH₃CH₂OH, water in the lattice is also involved. Figure S4 in the ESI contains representations for each of the complexes. The alternative environments are not expected to alter any exchange interaction between the centres as it is the triangular arrangement of the spins and the associated anisotropy which governs these processes.

Magnetic Properties

Polycrystalline samples of **1-4** were used for the collection of magnetic susceptibility data. DC measurements (2-300 K) in fields of 1 T (Figure 5) and 0.1 T (ESI Figure S5) gave similar results. The room temperature $\chi_M T$ values for complexes **1-4** are 40.6, 33.4, 39.6 and 34.0 cm³ mol⁻¹ K, respectively. The value obtained for **3** is consistent with the previous literature reports for a structural analogue (39.7 cm³ mol⁻¹ K).¹¹ At 300 K the μ_{eff} per Ln^{III} in complex **1-4** are 10.40, 9.43, 10.27 and 9.53 μ_B . These are consistent with the calculated

$g[J(J+1)]^{0.5}$ values of 10.65 (Dy³⁺), 9.72(Tb³⁺), 10.61 (Ho³⁺) and 9.58 (Er³⁺) μ_B per Ln centre. As the temperature is decreased from room temperature to about 100 K we see a slight decrease occurs in $\chi_M T$ that is likely the result of the depopulation of the excited Ln^{III} Stark

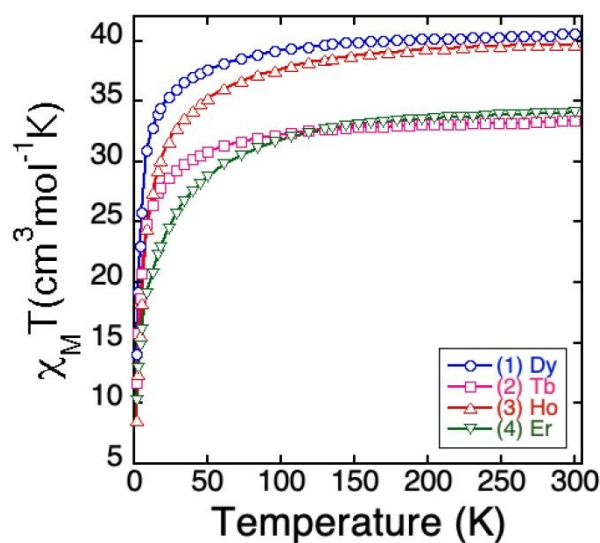


Figure 5: Temperature dependent $\chi_M T$ products in a DC field of 1 T for the series of [Ln₃(μ_3 -OH)₂(**o-dppd**)₃Cl₂L]²⁺ complexes, where Ln = Dy (**1**) blue; Tb (**2**) pink; Ho (**3**) red and Er (**4**) green.

levels. At lower temperatures, a more rapid decrease is observed, which is likely a result of the thermal depopulation of the low-lying Zeeman levels possibly combined with weak antiferromagnetic coupling between the centres.

Magnetisation (M) isotherms (2-20 K) for each of the complexes were determined in DC fields of 0 to 5 T. The results for **1** are shown in Figure 6 with similar results being observed for **2-4** (ESI Figure S6). In each of the complexes, the measurements made at 2 K do not reach a saturation value at 5 T (i.e. M has a value of 15.60, 13.64, 14.56 and 13.94 $N\beta$ for **1-4**, respectively). Similarly, a saturation in the magnetisation is not seen in 5 T fields at 3 K. The non-superimposability of the curves when plotted as M vs H/T supports the occurrence of low-lying levels that are energetically close to the ground state supporting the role of zero field splitting or Zeeman depopulation effects, arising from magnetic anisotropy. Despite the coordination environment being reminiscent of reported systems with a toroidal ground states, the shape of the M vs H plots at low fields does not have the S-shape that is often, but not always, associated with toroidal systems.^{15,18,20-22} However since these toroidal arrangements are influenced by molecular symmetry and the moment in addition to interaction one cannot rule out the possibility that there is a small energy gap between the nonmagnetic ground state and the first excited state which precludes the S-shape being observed.³⁴ At present *ab initio* calculations based on CASSCF method are best suited to identify such behaviour while experimental evidence would require methods such as micro-Squid magnetisation/hysteresis plots³¹ and NMR to unambiguously detect and describe such states.

Journal Name

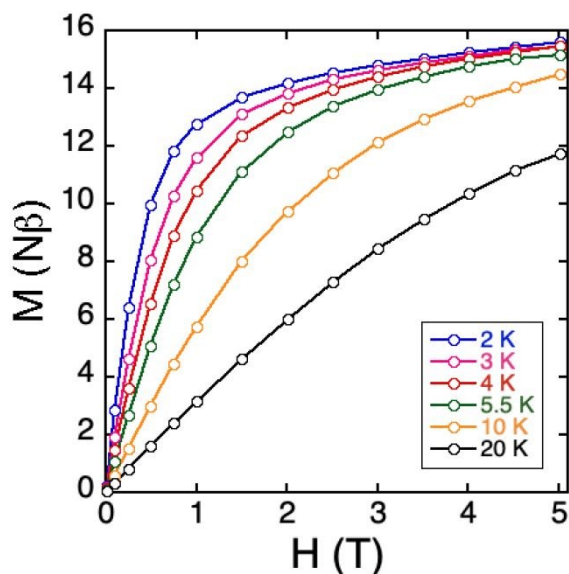


Figure 6: Magnetisation isotherms (2-20 K) in applied fields 0 to 5 T for complex 1.

Variable temperature (2-10 K) AC dynamic measurements were also undertaken for each of the complexes both with and without an applied bias DC field for a range of frequencies between 20 and 1488 Hz. The bias field applied in experiments was optimised for each sample by measuring changes χ_M'' in a static DC field under an applied oscillating field (1488 Hz and 498 Hz) at 3 K. The out of phase component, χ_M'' for the $[\text{Dy}_3(\text{OH})_2(\text{o-dppd})_3\text{Cl}_2(\text{H}_2\text{O})_4]$ complex is shown in Figure 7 in zero applied DC field. The Dy^{III} Kramer's ion complex **1** is found to have an out of phase signal below 8 K which varies with frequency. However, no maxima are observed in χ_M'' plots, even in an applied field (ESI Figure S7). Nevertheless, the signals are consistent with slow magnetic relaxation occurring for a multicentred Dy^{III} complex with insufficient anisotropy. The results for complexes **2-4** are given in the ESI (Figure S7). The DC fields applied in complexes **2-4** were used in an attempt to obtain efficient quantum tunnelling and, hopefully, observe frequency dependence of χ_M'' . However, a weak signal to noise (both with and without an applied DC field) was seen in the χ_M'' vs. temperature or vs. frequency plots for complexes **2-4** (ESI Figure S7), a result similar to cases involving Ln_6 toroids.³⁸ The χ_M'' vs. frequency log-plots for **2-4** showed that the weak, noisy data varied little upon applying the DC field (Figure S8) with no clear evidence for frequency dependent maxima. In the case of **1**, there is a hint of a maximum at ~ 1000 Hz, between 2-3 K, but a Debye analysis to estimate a U_{eff} value was not feasible.

Theoretical analysis

In the absence of the S-shape in the low temperature magnetisation isotherms, theoretical studies were undertaken to predict whether these systems have a toroidal spin arrangement. For a triangular Ln^{III} complex to display a toroidal spin arrangement, a planar arrangement of local anisotropy axes and the polynuclear Ln^{III} complex requires cyclic symmetry.³⁹

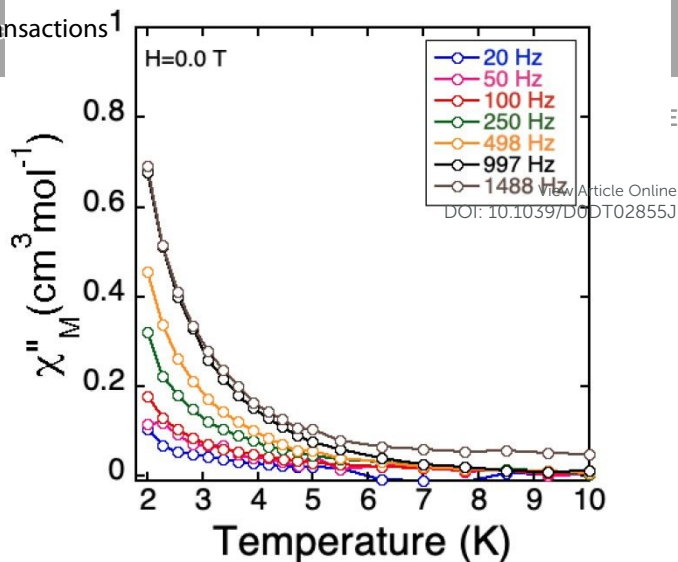


Figure 7: The temperature dependent (2-10 K) out of phase susceptibility, χ_M'' , for complex **1** in 0 T DC field.

Limitations of the MOLCAS packaged means calculations on the full complex **1** are not possible. Instead calculations were undertaken in two stages. Firstly, calculations are performed on each Dy centre by substitution of the other two Dy^{III} ions by diamagnetic Lu^{III} ions. Secondly, the single-ion anisotropy of all three Dy^{III} are combined together to understand the relaxation of the states. All calculations were performed using the X-ray crystal structure data as input.

The local g tensors for the low-lying Ising doublets in **2** and **3** and the Kramers doublets (KDs) for **1** and **4** are given in Tables S5-S9 in the ESI. The local g tensor for complexes **1-3** is Ising in nature with diminishing contribution towards the transverse anisotropy, as the combination of six O, one N and one Cl (for one centre seven O and one N) providing axial approach of ligand field around the oblate Ln^{III} ions in the eight coordinated square antiprism environment, whereas for the prolate Er ion, the g tensor is not axial in nature and they have significant transverse anisotropy.

Since the lanthanide centres are not completely symmetric to one another, the theoretical analysis confirms that, for the above ligand field environment when the oblate ion like Dy^{III} is approached by two different ligand from two different directions (keeping the other six coordination sites same), the Cl reduces the axiality compare to the O coordination. This is due to the increase in bond length for the former (around 2.54 Å) compared to 2.32 Å to the latter, which in response decreases the interaction of ligand with the metal centre.

For the complexes **1-4** the arrangement of each ground state anisotropy has been plotted (Figure 8) for all the Ln^{III} centres. In complex **1** the arrangement is in a circular pattern suggesting toroidal behaviour for the complex and the same is seen also in complex **3**. Interestingly in **2**, two of the Tb^{III} centres have the ground state anisotropy aligned along the triangular plan similar to **1** and **3**, however the g_{zz} axis of the Tb^{III} centre is perpendicular to the triangular plane, destroying the possible toroidal moments in this complex. This arises from the significant change in the coordination environment of Tb^{III} centre where in one water molecule is found coordinated trans to Cl position compared to ethanol coordination which is found in the other Tb^{III} centres. Hence the arrangement of anisotropic axis around the Tb^{III} centre is more or less

similar to that of complex **1** (Dy1 in Dy₃ complex), whereas the anisotropic axis for the Tb2 and Tb3 centres are parallel to each other. For the prolate Er^{III} ion, the ligand fields present are not suitable as they offer strong axial ligand and weaker equatorial ligation and this leads to significant transverse anisotropy at the ground state and hence no toroidal behaviour can be expected (Figure 8). Large transverse anisotropy arises due to significant mixing of the m_j states as shown in Figure S11 in ESI. The higher LoProp charge is present at the bridging O of the diketo group and less for the μ_3 -O and the terminal water O for all the complexes making the anisotropy axis lying in the direction of the bridging keto oxo group for the oblate ion complex **1-3** whereas for the prolate Er for complex **4**, the anisotropy axis moves away from above the diketo oxo group as shown in Figure 8.

The computed energy spectra for the low-lying Ising doublets for **2** and **3** or the KDs for complexes **1** and **4** are given in Tables S3 and S4 of ESI. From the Tables, one can clearly see that the Dy3 centre possessing two aqua ligands coordinated (and no -Cl) is found to have the largest ground-state excited state gap of 159 cm⁻¹ compared to other Dy centres (82 cm⁻¹ and 50 cm⁻¹ respectively

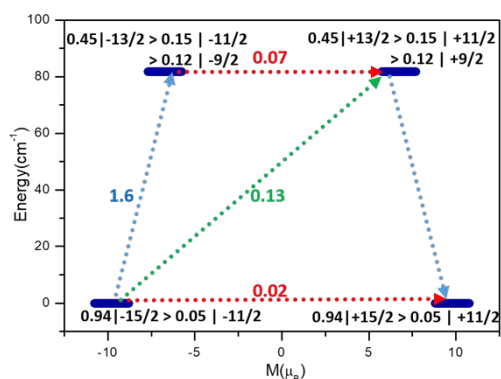


Figure 8: Dynamics for magnetic blocking relaxation through *ab initio* computation for Dy1. The thick blue line represents the Kramers doublets as a function of computed magnetic moment. The green dotted arrows show the possible pathway through Orbach/Raman relaxation, the dotted red lines and blue represent the presence of QTM/TA-QTM between the connecting pairs. The numbers provided at each arrow are the mean absolute value for the corresponding matrix element of transition magnetic moment. The numbers at the KDs represents the contribution of different states for the corresponding wave functions.

for Dy1 and Dy2). Moving to complexes **2** and **3**, for the Ising doublets, the tunnel splitting for complexes **2** and **3** occurs and is found to be in the range of 0.0005 to 0.1 cm⁻¹ for the former and in the range of 2 to 3 cm⁻¹ for the later which is in agreement with the previously reported molecule.¹¹ Due to the non-Kramers nature and high tunnel splitting it is very much expected that these molecules lack SMM behaviour and hence no significant peak for the out of phase susceptibility has been observed from the AC magnetic dynamics measurement.

In complex **4**, the ligand field is completely reversed to what is needed for the prolate ions. It is expected for complex **4** that slow relaxation will not be observed. Indeed this was confirmed from the experiments, where a large Quantum tunnelling of the magnetisation was found for all the three Er^{III} centres. For **1** there are

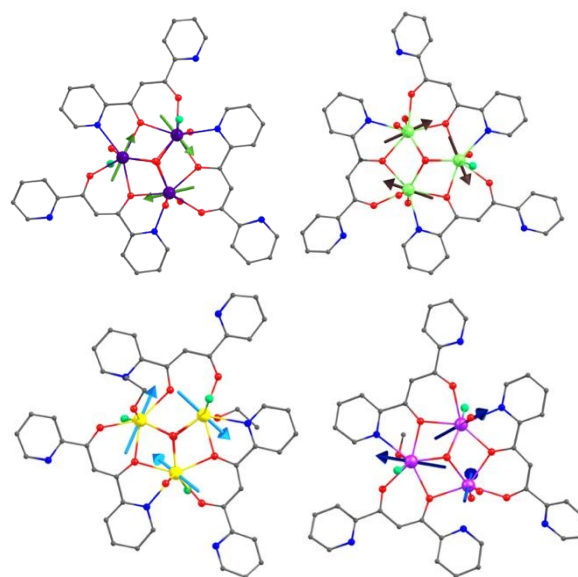


Figure 9: Arrangement of anisotropic axis for the ground state KDs and Ising doublets for complex **1-4**. Violet= Dy, green = Ho, Yellow= Tb, Pink= Er, Red= O, Grey= C, Blue= N, Green= Cl, H are omitted for clarity.

no clear maximum seen in the out of phase susceptibility plots, making it not possible to derive any relaxation time for magnetisation or magnetic blocking barrier. At the individual Dy^{III} centre, the ground state is not completely pure $m_j = \pm 15/2$ in nature with significant mixing from the excited m_j levels causing fast QTM between the degenerate ground state KDs. Moving from ground to first excited state the angle between the anisotropy axes for both states did not coincide with each other with very large angle of deviation causing the Raman and Orbach process between ground to first excited levels. The relaxation diagram for the individual lanthanide ions for Kramers ion are given in Figure 9 and ESI Figure S10 - S11.

Toroidal Behaviour and Exchange Coupling:

The inputs from the SINGLE_ANISO calculations have been used in the POLY_ANISO module to compute the exchange interactions between the Ln-Ln centre for all the four complexes and the energy levels for the exchange coupled state have been obtained. For calculating the exchange interaction, the Lines model has been taken into account with the Hamiltonian represented in the equations 1-3 (see below in Experimental). Since all the lanthanide centres are in distinctive ligand environments i.e. they have different terminal coordination, the exchange interactions between the Ln-Ln centres are expected to differ. We have considered three different exchange parameters for the three Ln centres represented in the Figure 10

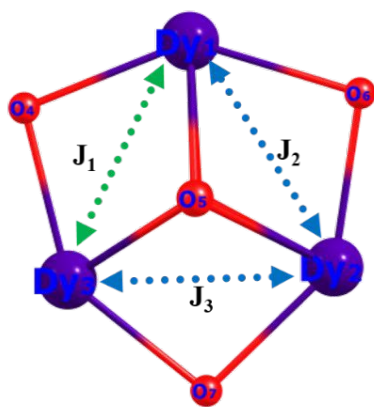


Figure 10: Mode of exchange between the Dy-Dy ions in complex 1.

below (see also ESI Figure S12). For complexes **2-4** all the three exchange interactions are found to be antiferromagnetic in nature as obtained by fitting both the experimental susceptibility and magnetisation data. For complex **1** there are two weak ferromagnetic and one weak antiferromagnetic exchange interactions. A closer look at the structure reveals that there are some differences in the geometrical parameters apart from the variation in the terminal ligand. Particularly one of $\mu_3\text{-OH}$, has significant asymmetry in Dy1-O(H)-Dy angles with one angle being slightly larger than the other two (98.05 vs. 97.15 and 96.45°). This large angle which corresponds to the J_1 interaction is between two Dy centres possessing terminal $-\text{Cl}$ ions. As shown earlier by us in magneto-structural correlations for several Dy2 dimers,^{40, 41} the angle here is at the border line where even a marginal change (approximately one degree) could switch the nature of exchange from weakly ferro to antiferromagnetic. These values are reflected in the bond angle analysis of the other three complexes as well. The corresponding Ln-O-Ln for the complex **2** are found to be 96.86, 96.95 and 96.42°, for complex **3** it was 97.78, 97.13 and 97.60°, and for complex **4**, 96.49, 96.43 and 97.06°. In all of these cases the magnetic interactions are found to be antiferromagnetic in nature. Moreover the smaller bond angles in complex **4** favours a greater antiferromagnetic contribution compared to the other complexes. The experimental and POLY_ANISO calculated temperature dependent $\chi_{\text{M}}T$ for complexes **1-4** are contained in the ESI in Figure S9.

Table 2 The exchange interactions between the Ln-Ln for complexes **1-4**; in cm^{-1} .

	J^1_{tot}	J^2_{tot}	J^3_{tot}	J^1_{exch}	J^2_{exch}	J^3_{exch}	J^1_{dipo}	J^2_{dipo}	J^3_{dipo}
1	-0.65	-0.05	-0.05	-0.25	-0.15	-0.15	-0.40	0.20	0.20
2	-0.16	-0.18	-0.18	-0.04	-0.06	-0.06	-0.12	-0.12	-0.12
3	-0.25	-0.23	-0.23	-0.10	-0.10	-0.10	-0.15	-0.13	-0.13
4	-1.95	-1.80	-1.80	-0.45	-0.40	-0.40	-1.50	-1.40	-1.40

From the SINGLE_ANISO calculations at the individual Ln centres it was found that in **1** and **3** there is a circular arrangement of the

ground state anisotropy which is responsible for the predicted toroidal moment. For these two complexes, the toroidal properties have been exploited using POLY_ANISO module^{42, 43} to obtain the toroidal states at the different energy levels. For this the magnetic interaction has been simulated by considering the magnetic dipole-dipole interaction and the exchange interaction explicitly within Lines model approximation. The Hamiltonian used for the approach is provided in the Experimental section, equations 1-3.

It has been observed that the flipping of spins occurs moving from the ground to first excited state causing switching to the reversal arrangement. The ground state vectors in **1** are found to be in almost perfect triangular arrangement where the angle of deviation of the g_z vector from the Dy₃ plane for complex **1** is 2.8°, 3.0° and 5.7° for Dy1, Dy2 and Dy3 respectively. Similarly for complex **3** these values are 3.9°, 1.5° and 1.9° for Ho1, Ho2 and Ho3 centres. The lack of toroidal behaviour for complexes **2** and **4** arises from the deviation of the g_z vector from the respective lanthanide Ln3 plane being too high. These values are 3.5°, 19.7° and 35.4° for complex **2**, whereas for complex **4**, no in plane vectors are found. The g_z is out of plane with respect to the Er₃ triangle.^{27, 30} The energy profile diagram is given in Figure 11.

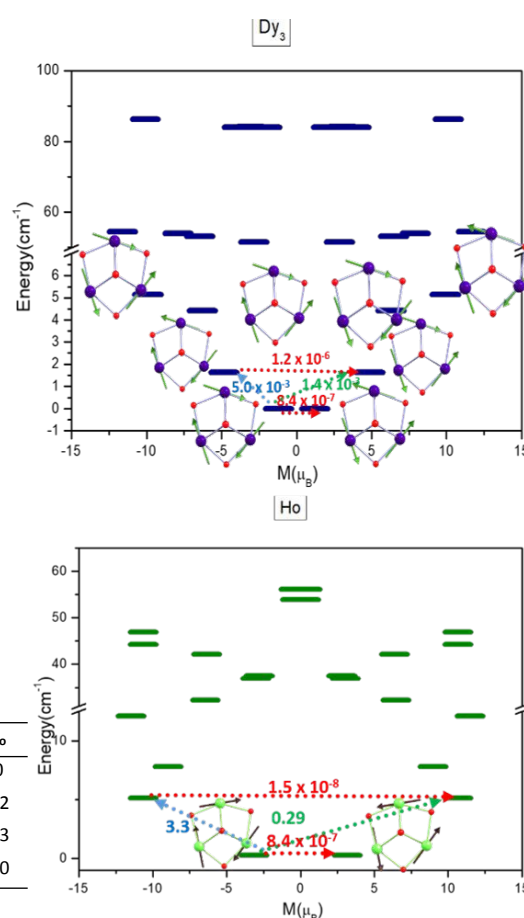


Figure 11: Low-lying exchange spectrum for complexes **1** (upper) and **3** (lower). The exchange coupled states (KDs) are placed on the diagram according to their magnetic moments (bold blue and green lines).

The ground toroidal state shows an energy difference of $\sim 1.6 \text{ cm}^{-1}$ to the first excited state where the flipping of one spin occurs (non-toroidal state). For complex **2** the anisotropy axes for the ground Ising doublet are similar to that of toroidal arrangement, (the angle has been reported above). However slight deviation of the g_z axis from the triangle plane and weaker coupling leads to smaller toroidal-non-toroidal state gap and hence a smaller barrier ($\sim 0.5 \text{ cm}^{-1}$) compared to complex **1**. In contrast, the axis for the complex **3** shows unusual behaviour due to the significant change in the terminal coordination for Tb-1 centre which we have already discussed above, causing two of the ground state axes to be parallel to each other. Moving to complex **4**, as a result of the prolate nature of the Er^{III} ion very large transverse anisotropy in the ground state was observed, and thus it is expected that there should not be any toroidal properties. This is confirmed from the theoretical studies.

Conclusions

Triangular arrangements of lanthanoid spins have been shown to exhibit a nonmagnetic ground state based on a vortex arrangement of spins. We have synthesised a family of trinuclear lanthanide complexes using pyridyl functionalised β -diketonate to investigate this phenomenon. The metal array has the general form $[\text{Ln}_3(\mu_3\text{-OH})_2(\text{o-dppd})_3\text{Cl}_x\text{L}_y]$ where $\text{Ln} = \text{Dy}^{\text{III}}, \text{Tb}^{\text{III}}, \text{Ho}^{\text{III}}$ or Er^{III} . We have undertaken magnetic studies and theoretical calculations on the complexes. Despite the inability to observe an S-shape at low temperatures and fields in the magnetisation isotherms, theoretical studies have predicted that complexes **1** and **3** support a toroidal spin arrangement. **1** is found to have a large ground state with Ising anisotropy, and the spins are arranged toroidally. Complex **3** is also predicted to show toroidal behaviour which is slightly inferior to **1**. For **2**, a large ground state anisotropy is present, but due to significant change in the coordination environment, it does not possess any toroidal behaviour. The inability to observe a flattening in the magnetic isotherms for these complexes is likely due to the nonmagnetic ground state which is not energetically well separated from the first excited state. Unsurprisingly, the prolate nature of Er in **4** and the large transverse anisotropy does not support a toroidal arrangement.

The Dy-Dy distance in **1** is similar (3.537 \AA to 3.553 \AA) to the previously reported Dy_3 toroidal molecule by Powell and co-workers²⁴ (3.514 to 3.540 \AA) and is shorter than another Dy_3 toroidal (Dy-Dy distance is 3.73 \AA) reported by Murray et al.³⁹ The angle between the ground state g_{zz} axis for **1** is found to be 6.13° , 10.6° and 2.7° for Dy1, Dy2 and Dy3 respectively and this is also similar to Powell's Dy_3 system (4.1° , 8.8° and 2.4°) and is significantly smaller than Dy_3 toroidal system report by Murray et al. ($\sim 12^\circ$). Due to the striking similarity of **1** to earlier Dy_3 system by Powell, we expect that their toroidal moments are comparable and is expected to be better than the Dy_3 system reported by Murray et al.

The present work confirms that a combination of both theoretical and experimental studies is essential in the determination of a toroidal state in triangular (and other) lanthanoid STMs.

Experimental

General

Unless otherwise stated, all reagents and solvents were purchased from Sigma Aldrich, Alfa Aesar and Combi-Blocks and used as received without further purification. The ligand **o-dppdH** and complex **3** were prepared according to previously published procedures.¹¹ Detailed synthetic procedures for all the products described in this work are reported in this section. Nuclear magnetic resonance spectra were recorded using a Bruker Advance 400 spectrometer (400 MHz for ^1H NMR; 100 MHz for ^{13}C NMR) at 300 K. All NMR spectra were calibrated to residual solvent signals. Infrared spectra were recorded using an attenuated total reflectance Perkin Elmer Spectrum 100 FT-IR with a diamond stage. IR spectra were recorded from $4000\text{--}650 \text{ cm}^{-1}$. Characterisation data (^1H NMR; ^{13}C NMR, IR) for the ligand are contained as figures within the ESI (pp 1-2). The intensity of the band is reported as strong (s), medium (m), or weak (w), with broad (br) bands also specified. Melting points were determined using a BI Barnsted Electrothermal 9100 apparatus. Elemental analyses were carried out on bulk samples using a Thermo Finning EA 1112 Series Flash. Inductively coupled plasma atomic emission spectroscopy (Murdoch-Marine and Freshwater Research Laboratory) was used to evaluate the lanthanoid content of the complexes. The metal analysis for the lanthanoid gave results consistent with the proposed formulations after extensive drying.

Crystallographic data for the structure were collected at 100(2) K on an Oxford Diffraction Gemini diffractometer with Mo $K\alpha$ or Cu $K\alpha$ radiation. Following absorption corrections and solution by direct methods, the structures were refined against F^2 with full-matrix least-squares using the program SHELXL-2014.⁴⁴ All hydrogen atoms were added at calculated positions and refined by use of riding models with isotropic displacement parameters based on those of the parent atoms. Anisotropic displacement parameters were employed throughout for the non-hydrogen atoms. Structure refinement data are reported in the SI.

1,3-bis(pyridin-2-yl)propane-1,3-dione (o-dppdH):

2-Acetylpyridine (5.60 mL, 0.050 mol) was dissolved in anhydrous THF (200 mL) and NaH (60% dispersion in paraffin oil, 2.40 g, 0.060 mol) was carefully added. Ethyl-2-picolinate (6.80 mL, 0.050 mol) was added dropwise and the mixture was vigorously stirred at 60°C for 12 hours. More portions of THF were added as the mixture thickened (30 mL x 2). The solvent was removed under reduced pressure and the red/orange solid was acidified in a 1:5 v/v glacial acetic acid:water solvent mixture. The solid was filtered out and washed with multiple portion of 1:5 v/v glacial acetic acid:water solvent mixture. The solid was then recrystallised from methanol. The target product was collected as an off-white powder. Yield: 6.16 g (54.5%). MP: $102\text{--}103^\circ\text{C}$. IR (ν / cm^{-1}): 3053 w (C-H asym stretch), 2922 w (C-H sym stretch), 1603 s (C=O stretch), 1317 m (C-N stretch). ^1H NMR (δ / ppm , $\text{DMSO-}d_6$): 8.77 (d, 2H, $J = 4.3 \text{ Hz}$), 8.20–7.94 (m, 6H), 7.64–7.62 (m, 2H). ^{13}C NMR (δ / ppm , $\text{DMSO-}d_6$): 196.6, 183.5, 151.9, 151.5, 149.7, 149.1, 137.7, 127.9, 127.2, 121.9, 121.5, 93.7, 48.1.

Anal. Calcd for **o-dppdH** C₁₃H₁₀N₂O₂: C 69.02, H 4.46, N 12.38%. Found: C 69.23, H 4.31, N 12.53%.

General synthesis for the lanthanide trinuclear clusters

o-dppdH (0.317 g, 0.0014 mol) was dissolved in dry methanol (40 mL) and triethylamine (0.2 mL) was added dropwise to deprotonate the diketone. LnCl₃·6H₂O (0.0007 mol) was added to the reaction mixture and heated at the reflux temperature for 48 hours. The solvent was evaporated under reduced pressure and the solid was dissolved in 40 mL of acetonitrile (to remove excess of ligand) and centrifuge for 5 minutes at 7500 rpm. The insoluble solid was retained and dissolved in 40 mL of pyridine, before being centrifuged again (unreacted lanthanoid salt precipitates out). The solution was collected and evaporated under reduced pressure and the solid was washed multiple times with diethyl ether (20 mL x 3). The target complex used for characterisation and magnetic measurements was either collected directly as a crystalline powder or recrystallised from methanol, ethanol or ethanol:hexanes mixture. With the exception of **2**, complexes have the general form [Ln₃(μ₃-OH)₂(o-dppd)₃Cl_xL_{6-x-y}L'_y]Cl_{4-x}, where: L and L' = H₂O or CH₃CH₂OH or CH₃OH. Metal analysis for the lanthanides gave results consistent with the proposed formulations. Elemental analysis was performed on bulk crystalline material.

[Dy₃(OH)₂(o-dppd)₃Cl₂(H₂O)₄]Cl₂·7H₂O (1**):** Yield: 0.210 g (19.7 %). Crystals suitable for X-ray analysis were obtained by slow evaporation of a methanol solution of the cluster over a week. MP: 323 °C (dec). IR (ν / cm⁻¹): 3195 w (OH stretch), 3005 w (C-H asym stretch), 2923 w (C-H sym stretch), 1521 s (C-O stretch), 1310 m (C-N stretch). Anal. Calcd for [Dy₃(OH)₂(C₁₃H₉N₂O₂)₃Cl₂(H₂O)₄](CH₃CH₂OH)₅=C₄₉H₆₇N₆O₁₇Cl₂Dy₃: C 37.47; H 4.30; N 5.35 %. Found: C 37.56; H 4.66; N 5.83 %. % Dy calculated 31.04 % found 31.9 %. μ_{eff}=10.40 B.M. per Dy³⁺.

{[Tb₃(o-dppd)₃(μ₃-OH)₂(CH₃CH₂OH)₃Cl₃][Tb₃(o-dppd)₃(μ₃-OH)₂(H₂O)(CH₃CH₂OH)₂Cl₃]Cl₂·H₂O} (2**):** Yield: 0.177 g (15.0 %). Crystals suitable for X-ray analysis were obtained by slow diffusion of hexane in an ethanol solution of the cluster over a week. MP: 318 °C (dec). IR (ν / cm⁻¹): 3183 w (OH stretch), 3005 w (C-H asym stretch), 2923 w (C-H sym stretch), 1520 s (C-O stretch), 1306 m (C-N stretch). Anal. Calcd for [Tb₃(C₁₃H₉N₂O₂)₃(OH)₂(H₂O)_{0.5}(CH₃CH₂OH)_{2.5}Cl₃](CH₃CH₂OH)₅H₅N = C₅₁H₅₆N₇O₁₂Cl₃Tb₃: C 39.72, H 3.66, N 6.35%. Found: C 39.41, H 3.67, N 6.35%. % Tb calculated 28.3 % found 28.7 %. μ_{eff}=9.43 B.M. per Tb³⁺.

[Ho₃(OH)₂(o-dppd)₃Cl(H₂O)₅]Cl₃·3H₂O (3**):** Yield: 0.181 g (16.8 %). Crystals suitable for X-ray analysis were obtained by slow evaporation of a methanol solution of the cluster over a week. MP: 314 °C (dec). IR (ν / cm⁻¹): 3375 w (OH stretch), 3053 w (C-H asym stretch), 2922 w (C-H sym stretch), 1521 s (C-O stretch), 1310 m (C-N stretch). Anal. Calcd for [Ho₃(OH)₂(C₁₃H₉N₂O₂)₃Cl(H₂O)₅](CH₃CH₂OH)₂(H₂O) = C₄₃H₅₃N₆O₁₆Ho₃Cl₃: C 34.17; H 3.53; N 5.56 %. Found: C 34.45; H 3.79; N 5.91 %. % Ho calculated 32.7 % found 32.9 %. μ_{eff}=10.27 B.M. per Ho³⁺.

[Er₃(OH)₂(o-dppd)₃Cl₂(H₂O)₃(CH₃OH)]Cl₂·3H₂O·CH₃OH (4**):** Yield: 0.155 g (12.3%). Crystals suitable for X-ray analysis were obtained by slow evaporation of a methanol solution of the cluster over a week. MP: 322 °C (dec). IR (ν / cm⁻¹): 3355 w (OH stretch), 3005 w (C-H asym stretch), 2923 w (C-H sym stretch), 1526 s (C-O stretch), 1312 m (C-N stretch). Anal. Calcd for [Er₃(OH)₂(C₁₃H₉N₂O₂)₃Cl₂(H₂O)₃(CH₃OH)]Cl₂(H₂O)(C₅H₅N)₂(CH₃CH₂OH)₃=C₅₆H₇₃Er₃N₈O₁₈Cl₄: C 37.40; H 4.26; N 6.65 %. Found: 37.49; H 4.30; N 6.86 %; % Er calculated 28.0 % found 27.4 %. μ_{eff}=9.53 B.M. per Er³⁺.

Crystallography

Experimental data for the structures were measured at 100(2) K on an Oxford Diffraction Gemini diffractometer or an Oxford Diffraction Xcalibur X-Ray diffractometers. In complexes **1**, **3**, **4** and **4a** the lattice Cl are disordered between several positions. During the refinement, their populations were forced to maintain a balance between the positively and negatively charged components of the complexes. The data were corrected for Lorentz and polarization effects and absorption. The structures were solved by direct methods and refined against *F*² with full-matrix least-squares using the programs SHELX.⁴⁵ Anisotropic displacement parameters were employed for the non-hydrogen atoms. All hydrogen atoms were added at calculated positions and refined by use of a riding model with isotropic displacement parameters based on those of the parent atom. Crystallographic data for the structures reported in this paper have been deposited at the Cambridge Crystallographic Data Centre. Copies of the data with CCDC numbers 2022326-2022330 can be obtained free of charge via <https://www.ccdc.cam.ac.uk/structures/>, or from the Cambridge Crystallographic Data Centre, 12 Union Road, Cambridge CB2 1EZ, U.KCB21EZ, UK (fax +441223336033; email deposit@ccdc.cam.ac.uk).

(1): C₃₉H₅₁Cl₄Dy₃N₆O₁₉, *M* = 1537.16, colourless needle, 0.192 × 0.048 × 0.028 mm³, triclinic, space group *P* $\bar{1}$ (No. 2), *a* = 10.1440(3), *b* = 17.5135(4), *c* = 17.9653(4) Å, α = 62.865(2), β = 73.868(2), γ = 78.120(2)°, *V* = 2716.81(13) Å³, *Z* = 2, *D*_c = 1.879 g cm⁻³, μ = 4.353 mm⁻¹. *F*₀₀₀ = 1490, MoKα radiation, λ = 0.71073 Å, 2θ_{max} = 64.5°, 58606 reflections collected, 17881 unique (*R*_{int} = 0.0847). Final *Goof* = 1.002, *R*₁ = 0.0613, *wR*₂ = 0.1201, *R* indices based on 10524 reflections with *I* > 2σ(*I*) (refinement on *F*²), |Δρ|_{max} = 2.5(2) e Å⁻³, 745 parameters, 133 restraints. CCDC-2022326

(2): C₈₈H₉₂Cl₈N₁₂O₂₃Tb₆, *M* = 2922.85, pale yellow blade, 0.291 × 0.119 × 0.030 mm³, triclinic, space group *P* $\bar{1}$ (No. 2), *a* = 13.3953(3), *b* = 14.2766(3), *c* = 14.9895(4) Å, α = 92.506(2), β = 97.712(2), γ = 95.225(2)°, *V* = 2824.30(12) Å³, *Z* = 1, *D*_c = 1.718 g cm⁻³, μ = 3.961 mm⁻¹. *F*₀₀₀ = 1414, MoKα radiation, λ = 0.71073 Å, 2θ_{max} = 64.7°, 61139 reflections collected, 18702 unique (*R*_{int} = 0.0516). Final *Goof* = 1.001, *R*₁ = 0.0458, *wR*₂ = 0.0987, *R* indices based on 13555 reflections with *I* > 2σ(*I*) (refinement on *F*²), |Δρ|_{max} = 0.25(2) e Å⁻³, 648 parameters, 10 restraints. CCDC-2022327

(3): C₃₉H₄₅Cl₄Ho₃N₆O₁₆, *M* = 1490.40, colourless block, 0.161 × 0.126 × 0.093 mm³, triclinic, space group *P* $\bar{1}$ (No. 2), *a* = 10.1060(6), *b* =

17.3501(9), $c = 18.1704(11)$ Å, $\alpha = 110.050(5)$, $\beta = 105.850(5)$, $\gamma = 101.302(4)^\circ$, $V = 2727.2(3)$ Å³, $Z = 2$, $D_c = 1.815$ g cm⁻³, $\mu = 10.157$ mm⁻¹. $F_{000} = 1436$, CuK α radiation, $\lambda = 1.54178$ Å, $2\theta_{\max} = 134.8^\circ$, 25032 reflections collected, 9622 unique ($R_{\text{int}} = 0.0769$). Final $\text{Goof} = 1.001$, $R1 = 0.0819$, $wR2 = 0.1944$, R indices based on 5808 reflections with $I > 2\sigma(I)$ (refinement on F^2), $|\Delta\rho|_{\max} = 1.4(2)$ e Å⁻³, 748 parameters, 177 restraints. CCDC-2022328

(4): C₄₁H₄₉Cl₄Er₃N₆O₁₆, $M = 1525.44$, pale brown needle, $0.272 \times 0.140 \times 0.056$ mm³, triclinic, space group $P\bar{1}$ (No. 2), $a = 10.0875(3)$, $b = 17.5576(4)$, $c = 18.0809(4)$ Å, $\alpha = 110.687(2)$, $\beta = 105.565(2)$, $\gamma = 100.854(2)^\circ$, $V = 2739.91(13)$ Å³, $Z = 2$, $D_c = 1.849$ g cm⁻³, $\mu = 4.814$ mm⁻¹. $F_{000} = 1474$, MoK α radiation, $\lambda = 0.71073$ Å, $2\theta_{\max} = 64.8^\circ$, 56013 reflections collected, 18104 unique ($R_{\text{int}} = 0.0284$). Final $\text{Goof} = 1.002$, $R1 = 0.0390$, $wR2 = 0.1024$, R indices based on 15201 reflections with $I > 2\sigma(I)$ (refinement on F^2), $|\Delta\rho|_{\max} = 4.3(2)$ e Å⁻³, 656 parameters, 40 restraints. CCDC-2022329

(4a): C₃₉H₄₇Cl₄Er₃N₆O₁₇, $M = 1515.40$, pale brown needle, $0.167 \times 0.111 \times 0.082$ mm³, triclinic, space group $P-1$ (No. 2), $a = 10.1697(2)$, $b = 17.4740(3)$, $c = 17.7993(3)$ Å, $\alpha = 62.933(2)$, $\beta = 74.798(2)$, $\gamma = 79.589(2)^\circ$, $V = 2711.1(1)$ Å³, $Z = 2$, $D_c = 1.856$ g cm⁻³, $\mu = 4.866$ mm⁻¹. $F_{000} = 1462$, MoK α radiation, $\lambda = 0.71073$ Å, $T = 100(2)$ K, $2\theta_{\max} = 65.7^\circ$, 61314 reflections collected, 18503 unique ($R_{\text{int}} = 0.0531$). Final $\text{Goof} = 1.003$, $R1 = 0.0521$, $wR2 = 0.1165$, R indices based on 12677 reflections with $I > 2\sigma(I)$ (refinement on F^2), $|\Delta\rho|_{\max} = 2.2(2)$ e Å⁻³, 634 parameters, 18 restraints. Lp and absorption corrections applied. CCDC-2022330

Magnetism

Magnetic susceptibility measurements were performed using a Quantum Design MPMS-XL 7 SQUID magnetometer. DC measurements were carried out at temperatures between 1.8 and 300 K in fields ranging from 0–5 T. AC susceptibility measurements were carried out in an oscillating ac field of 3.5 Oe and frequencies ranging from 0.1 to 1500 Hz. Measurements were made on polycrystalline samples contained in Vaseline to prevent torquing effects.

Computational Details

Theoretical investigation were performed using *ab initio* calculations based on the coordinates from the X-ray crystal structures with the MOLCAS 8.0 package.⁴⁶ The calculations involve the stepwise procedure of guessing the active orbitals followed by CASSCF and RASSI calculations.^{47, 48} Doughlass Kroll Hamiltonian has been included to take account of the relativistic effect which is more pronounced for the heavier lanthanide elements.⁴⁹ CASSCF calculations helps in achieving the spin free eigenstate. SINGLE_ANISO module is used to calculate the magnetic properties at individual lanthanide centre.⁵⁰ Using the inputs obtained from the SINGLE_ANISO module POLY_ANISO calculations has been done to plot the toroidal states as well the exchange interaction between the Ln-Ln centre. For the Ln ions TZVP level of basis set has been taken from the ANO...RCC library where as for the coordinated O and Cl TZV level of basis set has been used. For the remaining atoms DZV level basis has been used. We have employed the [ANO-RCC...

8s7p5d3f2g1h.] basis set for Ln^{III} atoms, the [ANO-RCC...3s2p.] basis set for C atoms, the [ANO-RCC...2s.] basis set for H atoms, the [ANO-RCC...3s2p1d.] basis set for N and O the [ANO-RCC...4s3p1d.] basis set for the Lu atom, [ANO-RCC...5s4p2d1f.] atoms. The Guessorb step involves for selecting the suitable active space, followed by the spin averaged CASSCF calculations. The active space taken for the Dy, Tb, Ho and Er are (9,7), (8,7), (10,7) and (11,7) respectively, indicating distribution of corresponding number of electrons in the seven 4f orbitals. For the configuration Interaction procedure 21 sextet roots has taken for Dy^{III}, for the Tb^{III} ion seven septet, one hundred and forty quintet excited states and one hundred and ninety-five triplet excited states for the Ho^{III} ion two hundred and ten triplet excited states and one hundred and ninety-five singlet excited states, for the Er^{III} ion thirty five quartet and one hundred twelve doublet excited states has been included. After computing all the excited state, all the low excited states (<50000 cm⁻¹) has been mixed through RASSI-SO module.⁴⁸ Finally the SINGLE_ANISO module helps in calculating the anisotropy factor of the low lying state as well as the nature of magnetic behaviour at individual Ln centre.

The above results gives the inputs for performing the POLY_ANISO module for the entire molecule to derive the exchange and dipolar interaction between the Ln-Ln centres. The Hamiltonian for calculating the exchange values has been given below.^{51, 52}

$$\hat{H}_{ex} = -\sum J_i S_i S_{i+1} \quad (1)$$

Here $J_i = J_{dip} + J_{exch}$; that is, J_i are the total magnetic interaction Ln-Ln, this describes the interaction between all the neighbouring metal centres.

$$\hat{H} = -\left(-J_{dip}^{Dy^i - Dy^{i+1}} + J_{exch}^{Dy^i - Dy^{i+1}}\right) \tilde{S}_{Dy^i} \tilde{S}_{Dy^{i+1}} \quad (2)$$

$$J_{dip}^{Dy^i - Dy^{i+1}} = \frac{\mu_B^2}{R_{Dy^i - Dy^{i+1}}^3} g_{Dy}^2 \quad (3)$$

Conflicts of interest

There are no conflicts to declare

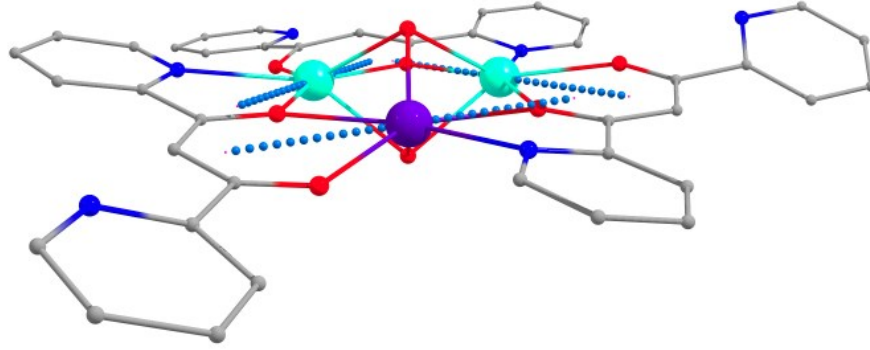
Acknowledgements

ROF thanks the ARC for a Discovery Early Career research Award (DE180100112). The authors acknowledge the CMCA Research Facility at UWA. KSM thanks the ARC for a Discovery grant. GR would like to than SERB and DST for funding (CRG/2018/000430; DST/SJF/CSA-03/2018-10; SB/SJF/2019-20/12). Dr Thomas Rodemann of the UTas Central Science Laboratory is thanked for elemental analysis.

References

1. J. Luzon and R. Sessoli, *Dalton Trans.*, 2012, **41**, 13556-13567.

2. R. Sessoli and A. K. Powell, *Coord. Chem. Rev.*, 2009, **253**, 2328-2341.
3. A. de Bettencourt-Dias, *Dalton Trans.*, 2007, 2229-2241.
4. B. L. Reid, S. Stagni, J. M. Malicka, M. Cocchi, G. S. Hanan, M. I. Ogden and M. Massi, *Chem. Commun.*, 2014, **50**, 11580-11582.
5. R. O. Fuller, G. A. Koutsantonis and M. I. Ogden, *Coord. Chem. Rev.*, 2020, **402**, 213066.
6. P. C. Andrews, W. J. Gee, P. C. Junk and M. Massi, *New J. Chem.*, 2013, **37**, 35-48.
7. N. F. Chilton, S. K. Langley, B. Moubaraki, A. Soncini, S. R. Batten and K. S. Murray, *Chem. Sci.*, 2013, **4**, 1719-1730.
8. S.-D. Jiang, B.-W. Wang, G. Su, Z.-M. Wang and S. Gao, *Angew. Chem. Int. Ed.*, 2010, **49**, 7448-7451.
9. D. Guettas, V. Montigaud, G. F. Garcia, P. Larini, O. Cador, B. Le Guennic and G. Pilet, *Eur. J. Inorg. Chem.*, 2018, **2018**, 333-339.
10. F. Pointillart, Y. Le Gal, S. Golhen, O. Cador and L. Ouahab, *Chem. Eur. J.*, 2011, **17**, 10397-10404.
11. P. C. Andrews, G. B. Deacon, R. Frank, B. H. Fraser, P. C. Junk, J. G. MacLellan, M. Massi, B. Moubaraki, K. S. Murray and M. Silberstein, *Eur. J. Inorg. Chem.*, 2009, 744-751.
12. P. C. Andrews, T. Beck, C. M. Forsyth, B. H. Fraser, P. C. Junk, M. Massi and P. W. Roesky, *Dalton Trans.*, 2007, 5651-5654.
13. S. K. Langley, N. F. Chilton, M. Massi, B. Moubaraki, K. J. Berry and K. S. Murray, *Dalton Trans.*, 2010, **39**, 7236-7249.
14. D. N. Woodruff, R. E. P. Winpenny and R. A. Layfield, *Chem. Rev.*, 2013, **113**, 5110-5148.
15. L. Rigamonti, A. Nava, M.-E. Boulon, J. Luzon, R. Sessoli and A. Cornia, *Chem. Eur. J.*, 2015, **21**, 12171-12180.
16. F.-S. Guo, B. M. Day, Y.-C. Chen, M.-L. Tong, A. Mansikkamäki and R. A. Layfield, *Science*, 2018, **362**, 1400.
17. C. A. P. Goodwin, F. Ortu, D. Reta, N. F. Chilton and D. P. Mills, *Nature*, 2017, **548**, 439-442.
18. D. D'Alessio, A. N. Sobolev, B. W. Skelton, R. O. Fuller, R. C. Woodward, N. A. Lengkeek, B. H. Fraser, M. Massi and M. I. Ogden, *J. Am. Chem. Soc.*, 2014, **136**, 15122-15125.
19. B. L. Reid, R. C. Woodward, R. O. Fuller, A. N. Sobolev, B. W. Skelton, M. I. Ogden and M. Massi, *J. Coord. Chem.*, 2016, **69**, 1852-1863.
20. L. F. Chibotaru, L. Ungur and A. Soncini, *Angew. Chem. Int. Ed.*, 2008, **47**, 4126-4129.
21. R. O. Fuller, K. L. Livesey, R. C. Woodward, A. J. McKinley, B. W. Skelton and G. A. Koutsantonis, *Aust. J. Chem.*, 2014, **67**, 1588-1594.
22. B. N. Figgis and G. B. Robertson, *Nature*, 1965, **205**, 694-695.
23. A. Figuerola, V. Tangoulis, J. Ribas, H. Hartl, I. Brüdgam, M. Maestro and C. Diaz, *Inorg. Chem.*, 2007, **46**, 11017-11024.
24. J. Tang, I. Hewitt, N. T. Madhu, G. Chastanet, W. Wernsdorfer, C. E. Anson, C. Benelli, R. Sessoli and A. K. Powell, *Angew. Chem. Int. Ed.*, 2006, **45**, 1729-1733.
25. H. Katsura, N. Nagaosa and A. V. Balatsky, *Phys. Rev. Lett.*, 2005, **95**, 057205.
26. A. Soncini and L. F. Chibotaru, *Phys. Rev. B*, 2010, **81**, 132403.
27. K. R. Vignesh, S. K. Langley, A. Swain, B. Moubaraki, M. Damjanović, W. Wernsdorfer, G. Rajaraman and K. S. Murray, *Angew. Chem. Int. Ed.*, 2018, **57**, 779-784.
28. S. Biswas, P. Kumar, A. Swain, T. Gupta, P. Kalita, S. Kundu, G. Rajaraman and V. Chandrasekhar, *Dalton Trans.*, 2019, **48**, 6421-6434.
29. J. Luzon, K. Bernot, I. J. Hewitt, C. E. Anson, A. K. Powell and R. Sessoli, *Phys. Rev. Lett.*, 2008, **100**, 247205.
30. S.-Y. Lin, W. Wernsdorfer, L. Ungur, A. K. Powell, Y.-N. Guo, J. Tang, L. Zhao, L. F. Chibotaru and H.-J. Zhang, *Angew. Chem. Int. Ed.*, 2012, **51**, 12767-12771.
31. K. R. Vignesh, A. Soncini, S. K. Langley, W. Wernsdorfer, K. S. Murray and G. Rajaraman, *Nat. Commun.*, 2017, **8**, 1023.
32. C. Das, S. Vaidya, T. Gupta, J. M. Frost, M. Righi, E. K. Brechin, M. Affronte, G. Rajaraman and M. Shanmugam, *Chem. Eur. J.*, 2015, **21**, 15639-15650.
33. L. Ungur, S. K. Langley, T. N. Hooper, B. Moubaraki, E. K. Brechin, K. S. Murray and L. F. Chibotaru, *J. Am. Chem. Soc.*, 2012, **134**, 18554-18557.
34. J. Lu, V. Montigaud, O. Cador, J. Wu, L. Zhao, X.-L. Li, M. Guo, B. Le Guennic and J. Tang, *Inorg. Chem.*, 2019, **58**, 11903-11911.
35. V. Montoya, J. Pons, X. Solans, M. Font-Bardia and J. Ros, *Inorg. Chim. Acta*, 2005, **358**, 2763-2769.
36. S. Alvarez, D. Avnir, M. Llunell and M. Pinsky, *New J. Chem.*, 2002, **26**, 996-1009.
37. S. K. Wolff, D. J. Grimwood, J. J. McKinnon, M. J. Turner, D. Jayatilaka and M.A. Spackman, *University of Western Australia*, 2012.
38. S. K. Langley, K. R. Vignesh, B. Moubaraki, G. Rajaraman and K. S. Murray, *Chem. Eur. J.*, 2019, **25**, 4156-4165.
39. S. K. Langley, K. R. Vignesh, T. Gupta, C. J. Gartshore, G. Rajaraman, C. M. Forsyth and K. S. Murray, *Dalton Trans.*, 2019, **48**, 15657-15667.
40. S. Mukherjee, J. Lu, G. Velmurugan, S. Singh, G. Rajaraman, J. Tang and S. K. Ghosh, *Inorg. Chem.*, 2016, **55**, 11283-11298.
41. T. Rajeshkumar, S. K. Singh and G. Rajaraman, *Polyhedron*, 2013, **52**, 1299-1305.
42. L. Ungur and L. F. Chibotaru, *POLY_ANISO program* 2007, KU Leuven:Belgium.
43. L. F. Chibotaru and L. Ungur, *The computer programs SINGLE_ANISO and POLY_ANISO*, 2006, University of Leuven, Belgium.
44. G. Sheldrick, *Acta Cryst. A*, 2008, **64**, 112-122.
45. G. Sheldrick, *Acta Cryst. C*, 2015, **71**, 3-8.
46. F. Aquilante, T. B. Pedersen, V. Veryazov and R. Lindh, *WIREs Computational Molecular Science*, 2013, **3**, 143-149.
47. P. Å. Malmqvist, B. O. Roos and B. Schimmelpfennig, *Chem. Phys. Lett.*, 2002, **357**, 230-240.
48. B. O. Roos and P.-Å. Malmqvist, *PCCP*, 2004, **6**, 2919-2927.
49. B. A. Heß, C. M. Marian, U. Wahlgren and O. Gropen, *Chem. Phys. Lett.*, 1996, **251**, 365-371.
50. L. F. Chibotaru and L. Ungur, *J. Chem. Phys.*, 2012, **137**, 064112.
51. L. Ungur, M. Thewissen, J.-P. Costes, W. Wernsdorfer and L. F. Chibotaru, *Inorg. Chem.*, 2013, **52**, 6328-6337.
52. S. K. Langley, D. P. Wielechowski, V. Vieru, N. F. Chilton, B. Moubaraki, B. F. Abrahams, L. F. Chibotaru and K. S. Murray, *Angew. Chem. Int. Ed.*, 2013, **52**, 12014-12019.



266x158mm (72 x 72 DPI)